The key role of yttrium oxide on devitrification resilience of barium gallo-germanate glasses: Physicochemical properties and crystallization study

Samar Aouji, Théo Guérineau, Rayan Zaiter, Evelyne Fargin, Younès Messaddeq, Thierry Cardinal

The key role of yttrium oxide on devitrification resilience of barium gallo-germanate glasses: Physicochemical properties and crystallization study

Samar Aouji [a,b,*], Théo Guérineau [b], Rayan Zaiter [a], Evelyne Fargin [a], Younès Messaddeq [b], Thierry Cardinal [a]

[a] Institut de Chimie de la Matière Condensée de Bordeaux, Université de Bordeaux, 87 Avenue du Dr Schweitzer, Pessac 33608, France
[b] Centre d'Optique, Photonique et Laser, Université Laval, 2375 Rue de la Terrasse, Québec G1V 0A6, Québec, Canada

Keywords:
Photonic
Heavy-metal oxide
Glass
Crystallization

A B S T R A C T

Two barium gallo-germanate glass series were elaborated to investigate the effect of the yttrium introduction on the glass physicochemical properties and crystallization behavior. One to twenty mol% of $YO_{3/2}$ were either added into the glass matrix or substituted for gallium oxide. The glass structure was studied by Raman spectroscopy and the thermal, optical, thermo-mechanical and physical properties are examined. The introduction of yttrium ions in both glass series increases the glass transition temperature, crystallization temperature, softening temperature, coefficient of linear thermal expansion and density. Through differential scanning calorimetry and X-ray diffraction analyses, it was found that competition occurs between the gallo-germanate zeolite-type phase and the yttrium-containing phase. From 13 mol% of $YO_{3/2}$, the yttrium introduction impedes the formation of surface crystallization in these glasses.

1. Introduction

Over the past decade, barium gallo-germanate (BGG) glasses have received increasing attention for the development of robust mid-infrared (MIR) optical fibers [1–5]. Indeed, BGG glasses not only have low phonon energy (≈ 830 cm^{-1}), but also high glass transition temperature (≈ 700 °C), high rare earth solubility (≈ 10^{21} ions/cm^3), and mechanical properties approaching those of silica in terms of elastic modulus (≈ 70 GPa) and hardness [5–13]. This combination of optical, thermal, and mechanical properties promises a bright future for the development of robust optical fibers operating in the mid-infrared range (up to 4.5 μm), making them prime candidates to compete with the most advanced soft glasses, i.e., fluoride, chalcogenide and tellurite glasses [5].

Core-cladding fibers made of soft glasses are usually produced from the preform-to-fiber process, in which a preform is made by the melt-quenching technique (including build-in-casting, rotational casting, rod-in-tube techniques, etc.) [14–18]. Although these preform fabrication techniques are easy to implement, the viscosity of the molten glass is a challenging parameter to control and monitor in order to achieve a good optical quality of the preform, a proper co-axiality and a smooth core-cladding interface, so that there are no defects and/or irregularities in the preform resulting in the formation of scattering elements and crystallization during the fiber drawing [19].

The fiber fabrication of BGG glasses from the preform-to-fiber process has faced a major problem of surface crystallization [4,13]. Compared to silica glasses, BGG glasses are characterized by a sharp working range due to the high slope of viscosity as a function of the temperature, in addition to the high softening temperature (≈ 675 °C) compared to the conventional soft glasses. Consequently, the application of standard manufacturing processes for core-cladding production remains laborious [4,13].

Initially, BGG fiber studies have been focused on understanding the surface crystallization origin and how it can be prevented by tailoring the glass composition [4,20,21]. Various chemical elements have been substituted or introduced into the BGG glass to avoid surface devitrification. Alkaline ions such as Na^+ and K^+ were substituted in the glass matrix, which increases the glass thermal stability ΔT (difference between the onset crystallization temperature T_x and glass transition temperature T_g), but also promotes surface crystallization during the preform-to-fiber process [4,21]. This glass surface devitrification was

* Corresponding author.
E-mail address: samar.aouji.1@ulaval.ca (S. Aouji).

https://doi.org/10.1016/XXXXXXXXXXXXXXXXXXXXXX

attributed to the high ionic mobility of the alkaline ions, compared to the other ions forming the glass system [21,22]. Wen et al.[1,2] showed the ability to draw a germanate optical fiber by incorporating rare-earth oxides, such as lanthanum and yttrium oxides, which are considered "anti-crystallization agents" in their studies. By adding these two rare-earths (RE), Wen et al. were able to produce a multimode and single-mode BGG fiber doped with Tm^{3+}. In their work, the addition of lanthanum and yttrium oxide leads to an increase in the glass transition temperature, refractive index, and thermal expansion coefficient. However, the mechanism responsible for the improved glass stability during fiber drawing has not yet been fully elucidated. However, this study encouraged researchers to concentrate their efforts on understanding the origins of surface crystallization and the key parameters for preventing it. These studies were initiated by Skopak et al. by studying the crystallization kinetics of the BaO - GeO_2 - $GaO_{3/2}$ – $KaO_{1/2}$ system [21]. They demonstrated a strong overlap between growth and nucleation phenomena, with the presence of two maximum temperatures for crystal growth, for which the first peak at 750 °C (below the fiber drawing temperature) corresponds to the surface growth of a zeolite-type phase such as $KaGaGeO_4$ and $BaGa_2O_4$. These observations were then underlined by the fiber drawing experiments of Guérineau et al., who also demonstrated the effectiveness of introducing an equimolar mixing ratio of lanthanum and yttrium cations. These studies enabled the fabrication of free-crystal fibers using the preform-to-fiber approach [4]. Since these results, work on fiber fabrication has continued. More recently, Calzavara et al. showed in their study of yttrium and lanthanum germano-gallate glasses that the addition of yttrium alone prevents surface crystallization compared with lanthanum, which promotes the formation of langasite-type crystalline [23]. This was subsequently confirmed by Zaiter et al. who succeeded in fabricating a mono-material fiber containing only yttrium and ytterbium cations [24].

To better understand the effect of RE introduction on BGG glass properties, the glass structure without any RE ions should first be clarified. It is a sequence of germanium and gallium tetrahedra connected by their corners, with barium ions balancing the negative charge of the gallium tetrahedra. The excess of barium ions that do not contribute to the gallium balancing mechanism depolymerize the gallo-germanate/germano-gallate glass network through the formation of non-bridging oxygens, preferentially on the germanate tetrahedra. However, few studies were conducted to understand the effects of RE ions such as lanthanum and yttrium on BGG glass structures, but also on their physicochemical properties [4,24–27].

First, Jewell et al. [25] investigated the effect of substituting gallium oxide for trivalent RE ions such as yttrium, gadolinium and lanthanum oxides. According to the authors, gadolinium and yttrium ions act both as glass modifiers due to their high field strength, which is defined as the ratio between the cation charge and cation-oxygen radius difference. However, these RE ions differ from other traditional glass modifiers such as alkali and alkaline-earth ions. Indeed, their incorporation into the glass structure leads preferentially to an increase in the glass transition temperature and the glass viscosity. In the meantime, lanthanum ion seems to rather play a dual role, by acting either as a gallium charge compensator or a network modifier. Studying gallo-germanate lanthanum glasses, Hwa et al. performed a structural study that may support this hypothesis. They suggest that the trivalent ion La^{3+} acts as a charge compensator, compensating the negative charge of gallium tetrahedra given the Ga/La ratio in their study, which is greater than one [28]. Recently, a similar study was performed by Calzavara et al. [27] on the dual role of lanthanum as a compensator and modifier in barium germano-gallate glasses as a function of Ga/Ge and (2Ba + 3La)/Ga ratios. Moreover, it should be mentioned that many crystalline phases are formed in the $GaO_{3/2}$ - GeO_2 - BaO - $LaO_{3/2}$ system. In such a case, the lanthanum introduction could destabilize the glass and favor a quick crystallization process. Finally, modified BGG compositions containing Tm, Yb, Ag, Bi, Ho, Gd and Ti glasses were recently investigated for optical properties, demonstrating the actual interest in bulk and fiber BGG glasses [11,22,24,29–32].

Recently, we have demonstrated the full potential of yttrium-stabilized BGG glass composition through the fabrication of the very first low-loss BGG optical fiber (about 200 $dB.km^{-1}$at 1350 nm) [19]. Hence, the purpose of our work is to investigate the effects of Y_2O_3 introduction either by addition or by gallium substitution on the physicochemical properties and crystallization behavior of barium gallo-germanate glasses. This article aims to clarify the ability of yttrium to produce BGG glass fibers without surface crystallization.

2. Experimental procedure

2.1. Materials preparation

The compositions are synthesized by a conventional melt-quenching method from gallium oxide Ga_2O_3 (Strem Chemical, 99.99%), germanium oxide GeO_2 (Strem Chemical, 99.999%), barium carbonate $BaCO_3$ (ACS Merck, 99%), and yttrium oxide Y_2O_3 (Strem Chemical 99.999%). The reactants are weighed, mixed, and then placed in a platinum crucible to be heated up at 1200 °C for 30 min and then melted at 1550–1600 °C for one hour under an ambient atmosphere. The molten glass is then quenched and annealed at 40 °C below the glass transition temperature, before being cut and optically polished.

2.2. Analytical method

The refractive indexes were measured by a prism coupling technique on a Metricon 2010/M apparatus at 532, 633, 972, 1308 and 1538 nm with an estimated error of ± 0.005.

The density of the glasses (ρ) was obtained by the Archimedes method at room temperature using the diethyl phthalate as immersion liquid and a Precisa XT 220A weighing scale with an estimated error of ± 0.01 $g.cm^{-3}$. The coefficient of linear thermal expansion (CTE), dilatometric softening point (T_d), and the dilatometric glass transition temperature (T_{gd}) were measured in a horizontal dilatometer NETZSCH TMA 402F1 between 25 et 830 °C under N_2 atmosphere at a heating rate of 5 $°C.m^{-1}$. The measurements were performed on cylindrical samples with two parallel faces having a 10 mm diameter and a height ranging between 6 and 10 mm. The dilatometric glass transition temperature (T_{gd}) is determined as the tangent inflection point, while the dilatometric softening temperature (T_d) corresponds to the peak temperature.

Glass viscosity curves obtained between 10^{10} and 10^7 Poise were recorded with a high-temperature Theta US parallel plate viscometer on the same samples used for dilatometry measurements. Under a load of 300 g, samples are heated up to the glass transition temperature at a rate of 4 $°C.min^{-1}$ then 2 $°C.min^{-1}$ up to 830 °C.

The glass transition (T_g), crystallization onset (T_x) and crystallization maximum (T_c) temperatures were measured by differential scanning calorimetry (DSC) with a Netzsch DSC Pegasus 404 PC apparatus on 100 mg glass powders introduced into a platinum crucible and heated at 10 $°C.min^{-1}$ up to 1100 °C. An N_2 flow was kept constant at 40 $ml.min^{-1}$. The thermal stability against crystallization ΔT of each composition is estimated using this equation:

$$\Delta T = T_x - T_g$$

The identification of crystallized phases was carried out by powder X-Ray Diffraction (XRD) patterns which were collected on a PANalitycalX'pert PRO MPD diffractometer in Bragg-Brentano θ-θ geometry equipped with a secondary monochromator and an X'Celerator multi-strip detector.

The Raman spectra were measured using a confocal Raman spectrometer LabRAM HR Evolution (Horiba Jobin Yvon) equipped with a Synapse CCD detector. Excitation was provided by a diode-pumped solid-state laser at 532 nm (output power of 20 mW). The incident laser beam was focused into the sample through a microscope with a

10X objective. The Raman intensity is multiplied by the Bose–Einstein correction factor, n_{BE}, to eliminate low wave number thermal:

$$n_{Bv} = 1 + \left(\exp\left(\frac{hv}{kT}\right) - 1\right)^{-1}$$

where ν is the frequency of the Raman shift, h is Plank's constant ($6.626.10^{-34}$ J.s), k the Boltzmann constant ($1.381.10^{-23}$ J.K^{-1}), and T the temperature of the Raman experiment. It's equal to 298 K for the spectra presented here.

3. Results

In this work, two yttrium-containing glass series are studied: one from the system 49 GeO_2 - (36 - x) $GaO_{3/2}$ - 15 BaO - $xYO_{3/2}$, where gallium is substituted by yttrium, namely S-xY. While the other is from the system (100 - x) (49 GeO_2 - 36 $GaO_{3/2}$ - 15 BaO) - $xYO_{3/2}$, where yttrium is added to the BGG matrix, namely A-xY. For both glass series x = 0, 6, 11, 13 and 15 mol%. The nominal glass compositions and the ratios 2Ba/Ga, Ga/Ge and Y/Ga are listed in Table 1. Chemical analysis of one of these compositions showed deviations of less than a few percent from the theoretical values. These deviations are probably due to measurement errors, indicating that there appears to be no evaporation in the glass compositions.

As reported in Fig. 1-(a) and (b), the density increases nonlinearly with the incorporation of yttrium in both glass systems from 4.44 g.cm^{-3} to 4.75 and 4.73 g.cm^{-3} for S-xY and A-xY glass series, respectively. In contrast to the density, the molar volume of the glasses evolves differently. In the S-xY compositions, the molar volume abruptly decreases from 29.69 cm^3.mol^{-1} to 28.92 cm^3.mol^{-1} from 0 to 6 mol% of yttrium. When the yttrium concentration increases up to 11 mol% and the 2Ba/G ratio is close to 1, i.e. there are enough barium ions to balance the negative charge of the gallium tetrahedra, the molar volume stabilizes. Above the yttrium concentration of 12 mol% and therefore in excess of barium ions, the molar volume decreases again to 28.48 cm^3.mol^{-1}. For the A-xY series, the molar volume seems to be constant as it slightly fluctuates between 29.9 cm^3.mol^{-1} and 29.5 cm^3.mol^{-1}. The density increases from 0 to 11 mol% and remains fairly constant above 10mol%.

The thermal and physical properties, including the glass transition temperature (T_g), the crystallization onset temperature (T_x), the maximum crystallization temperature (T_c), the thermal crystallization stability (ΔT), the coefficient of linear thermal expansion (CTE), the dilatometric glass transition temperature (T_{gd}) and the dilatometric softening point (T_d) are reported in Table2.

An increase in the values of the characteristic glass temperatures is observed when yttrium is introduced into both series. The glass transition temperature T_g rises from 654 °C to 729 °C and 732 °C in S-xY and A-xY, respectively, the onset temperatures T_x from 789 °C to 880 °C and 875 °C and the crystallization temperature T_c from 808 °C to 902 °C and 891 °C. The thermal glass stability against crystallization is always above 100 °C.

Table 1
Nominal compositions of the studied S-xY and A-xY glasses in cationic percentage (mol%) with the ratios 2Ba/Ga, Ga/Ge and Y/Ga.

	Cationic percentage (mol%)				Ratio		
Glass label	Ge^{4+}	Ba^{2+}	Ga^{3+}	Y^{3+}	2Ba/Ga	Ga/Ge	Y/Ga
0Y	49	15	36	0	0.8	0.7	0
S-6Y	49	15	30	6	1	0.6	0.2
S-11Y	49	15	25	11	1.2	0.5	0.4
S-13Y	49	15	23	13	1.3	0.5	0.6
S-15Y	49	15	21	15	1.5	0.4	0.7
A-6Y	46	14	34	6	0.8	0.7	0.2
A-11Y	44	13	32	11	0.8	0.7	0.3
A-13Y	43	13	31	13	0.8	0.7	0.4
A-15Y	42	13	31	15	0.8	0.7	0.5

In Fig. 2-(a), the entire DSC curves are depicted for both S-xY and A-xY series, while Fig.2-(b) and (c) highlight the crystallization region. Without yttrium, a single crystallization peak at 808 °C corresponding to a single crystalline phase is observed. As the concentration of yttrium is increasing in both series, this peak shifts at higher temperature while additional crystallization peaks are reported. Indeed, a second crystallization peak appears at 884 °C for S-6Y and 876 °C for A-6Y, indicating the formation of another crystalline phase. The second exothermic peak is more pronounced in A-6Y glass than in S-6Y. As the Y/Ga ratio increases, the second peak appears as a shoulder in A-11Y and A-13Y at 880 °C and 890 °C, respectively. In the S-xY system, the second exothermic peak is observed in S-13Y at 886 °C, while no second peak emerges in the S-11Y glass. For A-15Y sample, a single sharp crystallization peak forms at 891 °C, while a broad crystallization peak appears at 902 °C with a barely visible shoulder at 914 °C for its S-15Y counterpart.

As observed in Table 2 and Fig.3, the dilatometric glass transition temperature measured by TMA is relatively similar to the one measured by DSC, considering minor discrepancies. T_{gd} increases due to the introduction of yttrium into both glass series. The softening temperature and thermal expansion coefficient were performed in a temperature range between 25 °C and 830 °C. They both also increase with the increase of yttrium concentration from 692 °C to 765 °C and 748 °C, and from 7.2 10^{-6} °C^{-1} to 8.2 10^{-6} °C^{-1} and 7.8 10^{-6} °C^{-1} in S-xY and A-xY, respectively.

The viscosity evolution as a function of temperature is depicted in Fig. 4. The temperature varies from 750 °C to 900 °C with a viscosity ranging between $10^{10.2}$ and 10^6 Poise which corresponds to the softening interval [33]. The viscosity domain below $10^{7.5}$ was extrapolated from our measurements recorded at lower temperature as the viscosity evolve linearly in this range. For a same viscosity, the corresponding temperature is increasing in both S-xY and A-xY series. More specifically, for a viscosity of $10^{6.6}$ poise corresponding to the Littleton softening point, the temperature increases from 873 °C to 879 °C and 865 °C for S-15Y and A-15Y, respectively.

Figure 5 shows the refractive index dispersion of both series. The Sellmeier equation with a single oscillator is used to express the refractive index as a function of wavelength:

$$n^2(\lambda) = 1 + \frac{A\lambda^2}{\lambda^2 - B^2}$$

Where A and B are the material specific Sellmeier coefficients calculated after fitting the refractive indices at 532 nm, 633 nm, 972 nm, 1308 nm, and 1538 nm. The refractive index increases with the incorporation of yttrium into the matrix. Fig. 5 also highlights that the refractive indices of the A-xY glass system are higher than that of the S-xY one.

The unpolarized Raman spectra for both series are depicted in Fig.6. These Raman spectra can be divided into three regions: the low-frequency region between 200 cm^{-1} and 350 cm^{-1}, the mid-frequency region between 350 cm^{-1} and 650 cm^{-1}, and the high-frequency region between 650 cm^{-1} and 1000 cm^{-1}.

The mid-frequency region is attributed to the vibrational stretching-bending modes of T-O-T (T = Ge and/or Ga) oxygen bridging two germanium and/or gallium tetrahedra [26–29]. The main band at 510 cm^{-1} and the shoulder at 480 cm^{-1} are assigned to the stretching and bending vibration modes of the combined germanium and gallium tetrahedra, respectively. The bands in this region could also partially be assigned to the symmetric collective mode of regular rings, most likely four- and three-membered rings [34,35,37–39].

The high-frequency region and in particular the band around 850 cm^{-1} is assigned to localized symmetric and antisymmetric vibrational modes within the tetrahedral units of germanium with nonbridging oxygen (NBOs) called $Q^{n\ =1,\ 2,\ 3,\ 4}$ in which Q and n correspond respectively to tetrahedral germanium units and the number of oxygen bridging two germanium ions [39–41]. This region also includes the

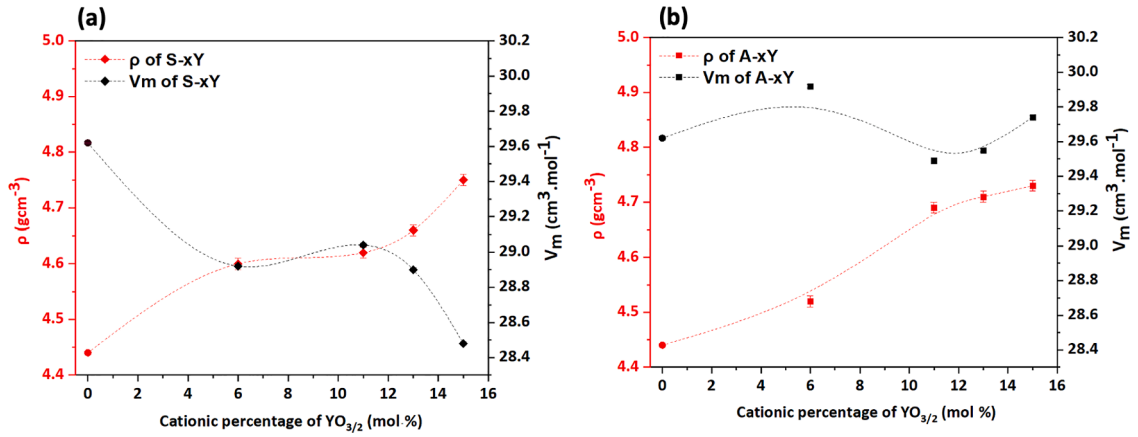

Fig. 1. (a), (b) the molar volume (V_m) and density (ρ) versus the cationic concentration of yttrium $YO_{3/2}$ (mol%) of the S-xY and A-xY glass system, respectively.

Table 2
Thermal and physical properties of the studied S-xY, and A-xY glasses: density (ρ), glass transition temperature (T_g), onset of crystallization temperature (T_x), maximum of crystallization (T_c), thermal stability (ΔT), coefficient of linear thermal expansion (CTE), the dilatometric glass transition temperature (T_{gd}) and the dilatometric softening point (T_d).

	Density	DSC					TMA		
Glass label	ρ (± 0.01 g.cm^{-3})	T_g (± 3 °C)	T_x (± 3 °C)	T_{c1} (± 3 °C)	T_{c2} (± 3 °C)	ΔT (± 6 °C)	CTE (± 0.0510^{-6} °C^{-1})	T_d (± 3 °C)	T_{gd} (± 3 °C)
0Y	4.44	654	789	808	–	135	7.2	692	656
S-6Y	4.59	696	820	842	884	124	7.2	714	679
S-11Y	4.62	700	856	882	–	156	7.7	724	700
S-13Y	4.66	713	838	865	886	125	7.9	748	712
S-15Y	4.75	729	880	902	914	151	8	765	728
A-6Y	4.52	683	821	847	876	138	7.3	718	683
A-11Y	4.69	711	843	871	880	132	7.4	724	701
A-13Y	4.71	725	855	875	890	130	7.4	746	712
A-15Y	4.73	732	875	891	–	143	7.8	748	713

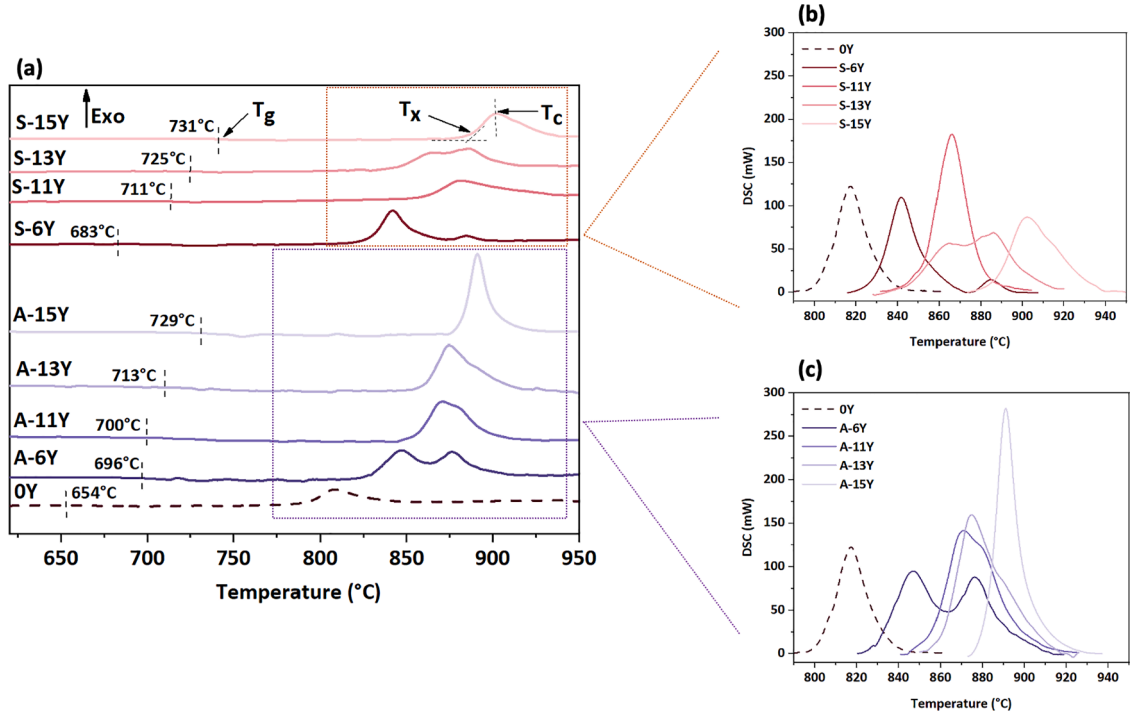

Fig. 2. (a) DSC curves for S-xY and A-xY series showing glass transition temperature (T_g), crystallization onset (T_x) temperature, and maximum crystallization temperature (T_c). Crystallization region is highlighted in (c) for S-xY and (d) for A-xY.

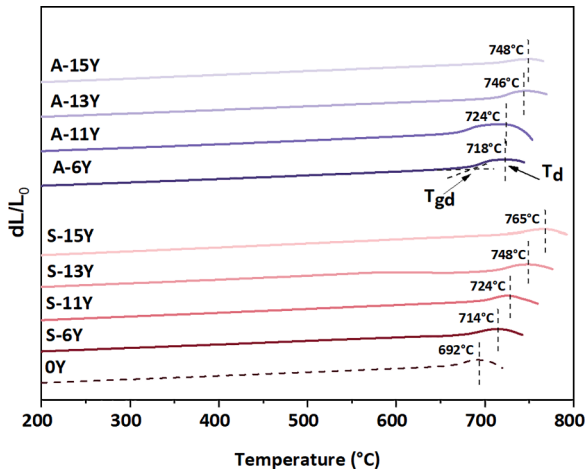

Fig. 3. TMA curves recorded for both S-xY and A-xY glass series. the measurements were performed in a temperature range between 25 °C and 830 °C.

stretching vibration at 785 cm^{-1} and 870 cm^{-1} of the mixed bonds ν (Ge-O^{-}-Ga) with an heterogeneous charge distribution on the oxygen ions [36].

The band at 510 cm^{-1} shifts to higher frequencies (at 520 cm^{-1} and 535 cm^{-1} in S-xY and A-xY series, respectively), as the yttrium concentration increases. In the meantime, the band peaking at 480 cm^{-1} decreases drastically in intensity, indicating the breaking of bonds between two germanium tetrahedra, and thus the formation of a complex glass structure. Focusing on the high-frequency region, when the 2Ba/Ga increase from 1 to 1.5 in the S-Yx glass system, two contributions appear at 755 cm^{-1} and 850 cm^{-1} in the form of a shoulder. Their intensity increases when the Y/Ga ratio increases from 0.2 to 0.7, until they become predominant compared to the other bands in this high-frequency region. According to the literature, the Raman bands at 755 cm^{-1} and 850 cm^{-1} are respectively attributed to the stretching vibration of germanium tetrahedra with two NBOs Q^2 and one NBOs Q^3 [35,38,39]. These two bands appear in the A-xY system, even though the 2Ba/Ga ratio is equal to 0.8, indicating that the yttrium participates in the depolymerization of the BGG lattice with increasing Y/Ga ratio. However, at the same yttrium concentration, these two bands are less intense than in the S-xY system.

An additional band is rising at 680 cm^{-1} when the Y/Ga ratio increases from 0.2 to 0.7. Some authors attributed this latter band to the edge-sharing octahedral germanium coordination site [36,42]. Meanwhile, Yashimoto et al. and Calzavara et al. attributed this band to the stretching mode of gallium coordination sites having a non-bridging oxygen [41,27]. It should be mentioned that this band can also be due

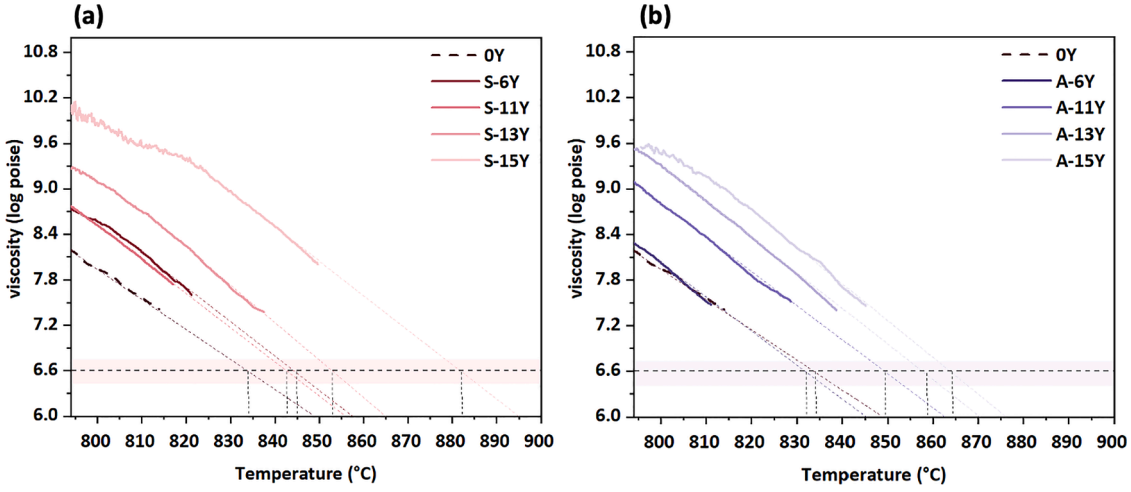

Fig. 4. The evolution of viscosity as a function of the temperature for (a) S-xY, and (b) A-xY. Solid lines represent the experimental data while dashed lines are their respective linear extrapolation.

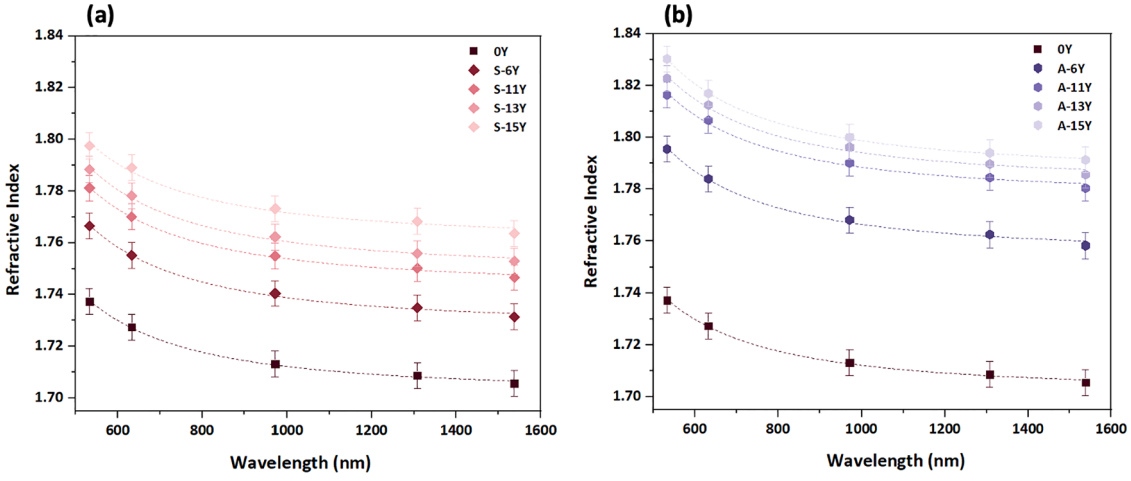

Fig. 5. Refractive index dispersion for (a) S-xY and (b) A-xY glasses.

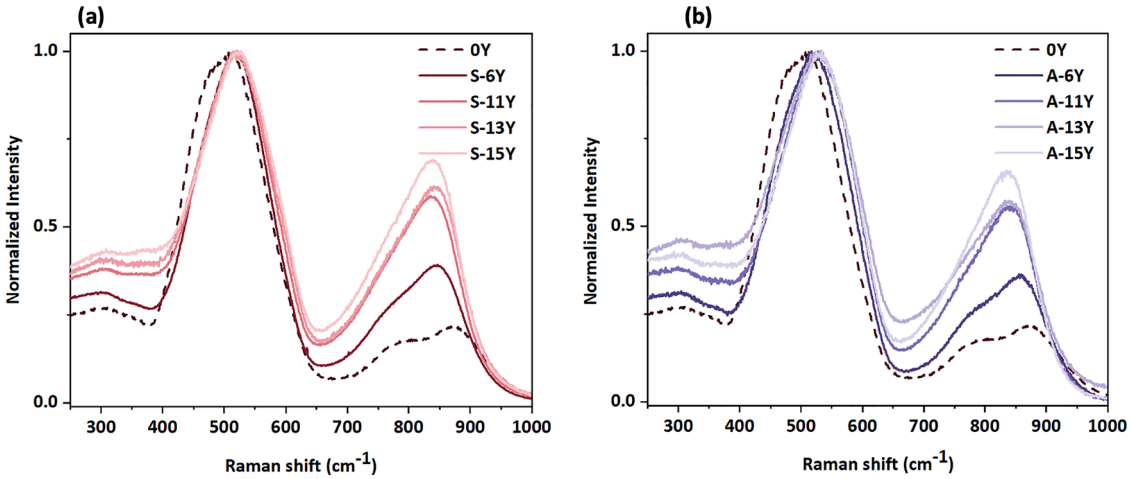

Fig. 6. Raman spectra of (a) S-xY, and (b) A-xY glasses normalized to the most intense band peaking at 500 cm^{-1}.

to bridges between different gallium ions [27].

The low-frequency region at 340 cm^{-1} is assigned to the localized vibration modes of modifier cations X - O, such as barium ions. According to the Raman spectra, a relative increase of this band is observed as the yttrium ions is introduced.

To study the crystallization kinetics and to determine the crystallized phases, four independent heat treatments were carried out at temperatures close to or above T_x: at 800 °C for 30 and 60 min, at 900 °C for 30 min, and at 940 °C for 30 min. Subsequently, the obtained samples were examined by X-ray diffraction (see Fig. 7-(a), (b) and (c)).

After the heat treatment performed at 800 °C for 30 min, only a broad signal with no diffraction peak is reported, suggesting that the glass samples are amorphous. At the same temperature but for 60 min (Fig.7-(a)), the germanate zeolite-type phase $BaGa_2Ge_2O_8$ (monoclinic) is detected with two different space groups P21/c (14) and C2/c [43, 44]. Both polymorphic phases were identified in the yttrium-free BGG glass, while only $P2_1/c$ (*) was identified in S-11Y, A-11Y and A-13Y samples. Additionally, regarding the diffraction peak intensity, the volume fraction of the $P2_1/c$ phase is higher in S-11Y than in A-13Y and A-11Y. Correlating this observation with the DSC results, the first crystallization peak in the DSC curve most likely corresponds to the nucleation and growth of $BaGa_2Ge_2O_8$, in which its volume fraction continues to increase with increasing heat treatment temperature up to 940 °C (see Fig. 7-(b) and c)). In the meantime, S-13Y, A-15Y and S-15Y samples remain amorphous even after prolonged heat treatment at 800 °C for 60 min (see Fig. 7-(a)). When the temperature increases up to 900 °C, both

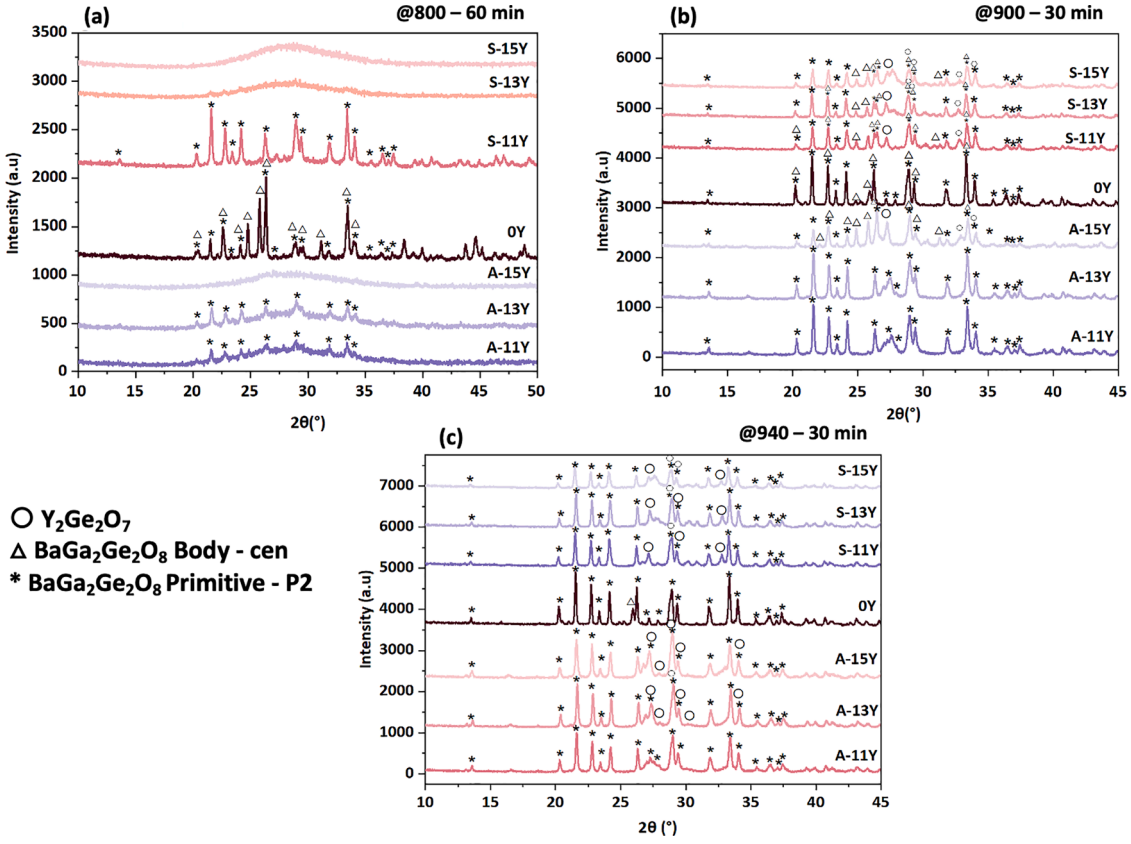

Fig. 7. X-ray diffractogram of 0Y, S-11Y, S-13Y, S-15Y, A-11Y, A-13Y and A-15Y glasses submitted to different heat treatments.

$BaGa_2Ge_2O_8$ polymorphs are detected in all S-xY samples. In the A-xY series, only $BaGa_2Ge_2O_8$ $P2_1/c$ was detected, except in A-15Y which contains both $BaGa_2Ge_2O_8$ polymorphs.

Moreover, an additional yttrium-containing phase, yttrium pyrogermanate $Y_2Ge_2O_7$ (○) [45,46], is formed as the heat treatment reaches 900 °C, except for A-13Y and A-11Y. After the 940 °C heat treatment, only A-11Y still does not present this yttrium crystalline phase. As reported in our DSC measurements, $Y_2Ge_2O_7$ seems to correspond to the second DSC crystallization peaks.

To investigate the relation between the viscosity at $10^{6.6}$ Poise (i.e., the Littleton softening point) and the crystallization kinetics in the S-xY series, heat treatment at 835, 843, 864 and 879 °C, on 0Y, S-11Y, S-13Y, and S-15Y, respectively was performed. As depicted in Fig. 8, both germanate zeolite-type phases ($BaGa_2Ge_2O_8$ $P2_1/c$ (*) and $BaGa_2Ge_2O_8$ C2/c (Δ)) and yttrium-containing phase, yttrium pyrogermanate ($Y_2Ge_2O_7$ (○)), are detected in the four glass samples. However, the characteristic peaks of the zeolite-type phases are more intense in 0Y and S-11Y than in the glasses with higher yttrium content, S-13Y and S-15Y.

4. Discussion

In general, the physical, thermal, and optical properties of a glass matrix are determined by the role and nature of the cations forming the network [47–49]. According to Raman analyses, germanium and gallium ions occupy tetrahedral sites in the form of $[GeO_4]$ and $[GaO_4]^-$, respectively. When the 2Ba/Ga ratio is ≈ 1, the glass matrix consists of a sequence of germanium and gallium polyhedral connected by their corners [21], with a sufficient Ba^{2+} quantity to balance the negative charge of the gallium tetrahedra. When the ratio 2Ba/Ga is greater than 1, the Ba^{2+} ions are in excess, leading to the formation of NBOs on the germanium tetrahedra [39,36]. When the 2Ba/Ga ratio is inferior to 1, the Ba^{2+} ions are not enough to compensate for the negative charge of the $[GaO_4]^-$ tetrahedra. The gallium units are expected to change their coordination from 4 to 5 and/or 6 [15,29]. The presence of mixed bonds Ge-O^--Ga is quite conspicuous in the 0Y glass, reflected in the bands at 785 cm^{-1} and 872 cm^{-1} attributed to the stretching vibration of ν (Ge - O^- - Ga) [36]. When gallium is replaced for yttrium, the Ga/Ge ratio decreases from 0.7 to 0.3, leading to a transition from a gallo-germanate glass system to an yttrio-germanate glass system. Those structure modifications induced a shift of the 510 cm^{-1} band to high frequencies. The same observation is reported also in Calzavara et al. study [27]. However, it's difficult in Raman to distinguish the vibrational modes of T-O-T because the two atoms have similar mass and coordination.

Increasing the Y/Ga ratio leads to a decrease in the gallo-germanate network polymerization in both glass systems. Indeed, The Raman spectra reveal that the peaks assigned to the vibrational modes of Q^2 and Q^3 of both gallium and/or germanium tetrahedra are substantially increased compared to the T-O-T bands. Moreover, when yttrium is added to the matrix, it noticeably increases the T_g, density, and viscosity, which tends to confirm that the yttrium is involved in the glass network and cannot be considered only as a glass modifier.

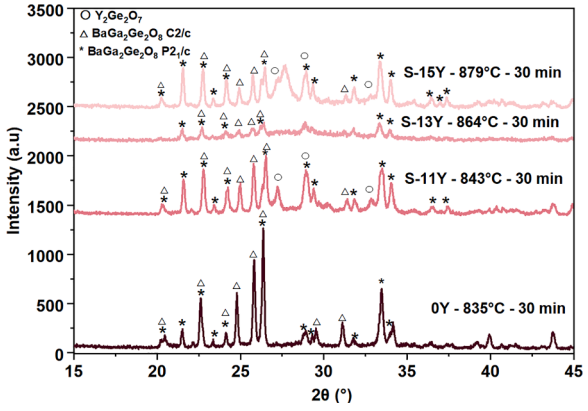

Fig. 8. X-ray diffractogram of 0Y, S-11Y, S–13Y and S-15Y glasses submitted to heat treatment at the Littleton point.

This type of structural and properties changes have also been observed in boron and aluminosilicate glasses where $AlO_{3/2}$ has been replaced by yttrium or added to the glass matrix [50–61] and in germanate-silica glasses [62]. These studies rely on their interpretations of yttrium's field strength and coordination number. According to the Diezel criteria [63], the role of a cation in a glassy network is characterized by the Colombian attraction force or the field strength A, which is defined as the ratio between the cationic charge Z_c and the ionic radius between the cation r_c and oxygen r_o:

$$A = \frac{Z_c}{(r_c + r_o)^2}$$

Based on these previous studies and the results of the present work, the change observed in BGG glasses was interpreted as follows: Y^{3+} has a higher field strength [25] compared to Ba^{2+}, while it is larger than Ga^{3+}. Its intermediate nature differentiates it from Ba^{2+}(+II) as a simple modifier or compensator ion. In addition to its high field strength, Y^{3+} probably also has a high coordination number, greater than or equal to 6 [64]. When $Y^{3+}$is incorporated into the network, it can connect the gallium and/or germanium tetrahedra, making the glass network more compact and rigid as the Y/Ga ratio increases [64]. As a result, the density, glass transition temperature and viscosity increase with the increase of $YO_{3/2}$ content. This was also observed by Jewell et al. in their study on gallo-germanate, while they were added a small amount of yttrium in their study compared to our present work.

The appearance of a new band at about 680 cm^{-1} with increasing yttrium concentration also indicates a significant change in the glass structure. Again, the correlation can be established with the structural change occurring in aluminosilicate glasses when the yttrium is introduced into the glass matrix. Indeed, various experimental techniques such as X-ray and neutron diffraction, NMR [64–67], molecular dynamics simulations, FTIR and Raman spectroscopies [68] have demonstrated that the abundance of higher coordinated aluminum units increases as the Y/Al ratio increases. it suggests that yttrium ions promote the conversion of 4-coordinated aluminum to higher coordinated structural units, leading to severe deformations of the matrix with the formation of polyhedral edge-sharing in addition to corner-sharing [66, 67].

The density values, which do not evolve linearly with the yttrium oxide concentration, present a clear gap between the value measured below 6 mol% and above 11 mol% of $YO_{3/2}$. This evolution versus the yttrium content coincides in the Raman spectra with the appearance of NBOs on the germanium tetrahedra. This new environment in the BGG glass could also explain the slowdown in the formation of the zeolite-type phase $BaGa_2Ge_2O_8$, as it may limit the ion diffusion and migration during heat treatment.

In alumino-silicate glasses, it has also been demonstrated that the yttrium in alkali and alkaline aluminosilicate glasses strongly affects the crystallization process. Kang et al. [55] reported in glasses from the MgO - $AlO_{3/2}$ - SiO_2 system that a concentration of 2 mol% of $YO_{3/2}$ inhibits the crystallization process and forces the quartz solid solution (yttrium-free crystalline phase) to be form at higher temperatures. Dittmer et al. [58] found that the use of 4 mol% of $YO_{3/2}$ prevents the precipitation of the α-quartz solid solution in the MgO - $AlO_{3/2}$ - SiO_2 - ZrO_2 system. Singh et al. [69] showed in SiO_2 – MgO - $BO_{3/2}$ - $AlO_{3/2}$ glasses that increasing the yttrium concentration up to 6 mol% leads to the crystallization of Mg_2SiO_4 and $MgSiO_3$ instead of cordierite phase ($Mg_2Al_4Si_5O_{18}$).

In our study, a clear competition between the zeolite-type phases and the yttrium pyrogermanate phase $Y_2Ge_2O_7$ has been revealed for heat

treatments at 900 and 940 °C. Indeed, we report that yttrium acts as a retarder and its incorporation impedes the formation of the zeolite-type phase responsible for BGG surface crystallization.

5. Conclusion

The introduction effect of 1 to 20 mol% of $YO_{3/2}$ on the properties and crystallization behavior of BGG glasses was studied. The structure is initially a three-dimensional network consisting of alternating germanium and gallium tetrahedra connected by the corners. The negative charge of the gallium tetrahedra is compensated by the barium ions. When yttrium is added to the glass matrix, the structure becomes more compact, increasing the T_g, density, coefficient of thermal expansion, and viscosity, while generating non-bridging oxygens on the germanium and/or gallium tetrahedra. This impact is predominantly attributed to the large field strength of the yttrium compared to the barium. Finally, it also affects the crystallization kinetics of BGG glass, by impeding the crystallization process and the formation of the gallo-germanate zeolite-type phase while promoting yttrium-containing phases.

CRediT authorship contribution statement

Samar Aouji: Conceptualization, Validation, Investigation, Writing – original draft, Writing – review & editing. **Théo Guérineau:** Validation, Supervision, Writing – review & editing. **Rayan Zaiter:** Validation, Writing – review & editing. **Evelyne Fargin:** Supervision, Funding acquisition, Writing – review & editing. **Younès Messaddeq:** Validation, Supervision, Funding acquisition, Project administration, Writing – review & editing. **Thierry Cardinal:** Validation, Supervision, Funding acquisition, Project administration, Writing – review & editing.

Declaration of Competing Interest

The authors declare the following financial interests/personal relationships which may be considered as potential competing interests: Thierry Cardinal reports financial support was provided by Region Nouvelle-Aquitaine. AOUJI Samar reports financial support was provided by FUNGLASS. AOUJI Samar reports financial support was provided by Mitacs Canada. Theo Guerineau reports was provided by Sentinel North. Younes Messaddeq reports financial support was provided by Canadian Research Chair program. non

Data availability

No data was used for the research described in the article.

Acknowledgments

This research was supported by Agence Nationale de la Recherche (ANR) (ANR-18-CE08–0004–02) and the New Aquitaine Region (2018–1R10127). This project has received funding from the European Union's Horizon 2020 research and innovation program under the Marie Skłodowska-Curie grant agreement No 823941 (FUNGLASS), as well as the Mitacs Globalink program.

This work has received also funding from the Canadian Government, managed by Sentinel North program of the University Laval and the Canadian Research Chair program (CERC).

References

[1] X. Wen, G. Tang, J. Wang, X. Chen, Q. Qian, Z. Yang, Tmˆ3+ doped barium Gallo-Germanate glass single-mode fibers for 20 Mm laser, Opt. Express 23 (6) (2015) 7722, https://doi.org/10.1364/OE.23.007722.

[2] X. Wen, G. Tang, Q. Yang, X. Chen, Q. Qian, Q. Zhang, Z. Yang, Highly Tm3+ doped Germanate glass and its single mode fiber for 2.0 Mm laser, Sci. Rep. 6 (1) (2016) 20344, https://doi.org/10.1038/srep20344.

[3] M. Kochanowicz, J. Zmojda, P. Miluski, A. Baranowska, M. Leich, A. Schwuchow, M. Jäger, M. Kuwik, J. Pisarska, W.A. Pisarski, D. Dorosz, Tm $^{3+}$ /Ho $^{3+}$ Co-doped germanate glass and double-clad optical fiber for broadband emission and lasing above 2 Mm, Opt. Mater. Express 9 (3) (2019) 1450, https://doi.org/10.1364/OME.9.001450.

[4] T. Guérineau, C. Strutynski, T. Skopak, S. Morency, A. Hanafi, F. Calzavara, Y. Ledemi, S. Danto, T. Cardinal, Y. Messaddeq, E. Fargin, Extended Germano-gallate fiber drawing domain: from germanates to gallates optical fibers, Opt. Mater. Express 9 (6) (2019) 2437, https://doi.org/10.1364/OME.9.002437.

[5] C. Strutynski, F. Calzavara, T. Guerineau, L. Loi, R. Laberdesque, J.-M. Rampnoux, S. Morency, Y. Ledemi, Y. Petit, M. Dussauze, F. Désévédavy, F. Smektala, S. Danto, L. Canioni, Y. Messaddeq, E. Fargin, T. Cardinal, Heavy-oxide glasses with superior mechanical assets for nonlinear fiber applications in the mid-infrared, Opt. Mater. Express 11 (5) (2021) 1420, https://doi.org/10.1364/OME.417699.

[6] P.L. Higby, I.D. Aggarwal, Properties of barium gallium germanate glasses, J. Non-Cryst. Solids 163 (3) (1993) 303–308, https://doi.org/10.1016/0022-3093(93)91308-P.

[7] J.M. Jewell, I.D. Aggarwal, Structural influences on the hydroxyl spectra of barium gallogermanate glasses, J. Non-Cryst. Solids 181 (1–2) (1995) 189–199, https://doi.org/10.1016/0022-3093(94)00471-4.

[8] Bayya, S.S.; Chin, G.D.; Sanghera, J.S.; Aggarwal, I.D. VIS-IR Transmitting BGG Glass Windows; Tustison, R. W., Ed.; Orlando, FL, 2003; p 208. https://doi.org/10.1117/12.487723.

[9] P.L. Higby, C.I. Merzbacher, I.D. Aggarwal, E.J. Friebele, Gallogermanate glasses as near IR optical waveguides, MRS Proc 244 (1991) 115, https://doi.org/10.1557/PROC-244-115.

[10] S.S. Bayya, G.D. Chin, J.S. Sanghera, I.D. Aggarwal, J.A. Detrio, Thermo-optic coefficient of barium gallogermanate glass, Appl. Opt. 46 (32) (2007) 7889, https://doi.org/10.1364/AO.46.007889.

[11] R.F. Falci, T. Guérineau, J.-L. Delarosbil, Y. Messaddeq, Spectroscopic properties of gallium-rich germano-gallate glasses doped with Tm3+, J. Lumin 249 (2022), 119014 https://doi.org/10.1016/j.jlumin.2022.119014.

[12] H. Lin, X.Y. Wang, C.M. Li, H.X. Yang, E.Y.B. Pun, S. Tanabe, Near-infrared emissions and quantum efficiencies in Tm3+-doped heavy metal gallate glasses for S- and U-band amplifiers and 1.8μm infrared laser, J. Lumin. 128 (1) (2008) 74–80, https://doi.org/10.1016/j.jlumin.2007.05.015.

[13] Skopak, T. Elaboration et caractérisation de verres et fibres optiques à base d'oxyde de gallium pour la transmission étendue dans l'infrarouge. 2017, 308.

[14] G. Tao, H. Ebendorff-Heidepriem, A.M. Stolyarov, S. Danto, J.V. Badding, Y. Fink, J. Ballato, A.F. Abouraddy, Infrared fibers, Adv. Opt. Photon. 7 (2) (2015) 379, https://doi.org/10.1364/AOP.7.000379.

[15] W.C. Wang, B. Zhou, S.H. Xu, Z.M. Yang, Q.Y. Zhang, Recent advances in soft optical glass fiber and fiber lasers, Prog. Mater. Sci. 101 (2019) 90–171, https://doi.org/10.1016/j.pmatsci.2018.11.003.

[16] M. Poulain, S. Cozic, J.L. Adam, Fluoride glass and optical fiber fabrication. Mid-Infrared Fiber Photonics, Elsevier, 2022, pp. 47–109, https://doi.org/10.1016/B978-0-12-818017-4.00009-4.

[17] J.A. Harrington, Infrared Fibers and Their Applications, SPIE Optical Engineering Press, Bellingham, Wash, 2004.

[18] H. Ebendorff-Heidepriem, P. Wang, Oxide glass and optical fiber fabrication. Mid-Infrared Fiber Photonics, Elsevier, 2022, pp. 111–176, https://doi.org/10.1016/B978-0-12-818017-4.00001-X.

[19] T. Guérineau, S. Aouji, S. Morency, F. Calzavara, P. Larochelle, P. Labranche, J. Lapointe, S. Danto, T. Cardinal, E. Fargin, M. Bernier, R. Vallée, Y. Messaddeq, Toward low-loss mid-infrared Ga2O3–BaO–GeO2 optical fibers, Sci. Rep. 13 (1) (2023) 3697, https://doi.org/10.1038/s41598-023-30522-1.

[20] P. Hee. Exploration de Nouvelles Générations de Verres de Gallates Pour La Photonique, 2014, p. 248.

[21] T. Skopak, F. Calzavara, Y. Ledemi, F. Célarié, M. Allix, E. Véron, M. Dussauze, T. Cardinal, E. Fargin, Y.Properties Messaddeq, Structure and crystallization study of germano-gallate glasses in the Ga2O3-GeO2-BaO-K2O system, J. Non-Cryst. Solids 514 (2019) 98–107, https://doi.org/10.1016/j.jnoncrysol.2019.02.028.

[22] T. Guérineau, A. Fargues, Y. Petit, E. Fargin, T. Cardinal, The influence of potassium substitution for barium on the structure and property of silver-doped germano-gallate glasses, J. Non-Cryst. Solids 566 (2021), 120889, https://doi.org/10.1016/j.jnoncrysol.2021.120889.

[23] F. Calzavara, P. Florian, F. Fayon, V. Sarou-Kanian, T. Guérineau, S. Danto, Y. Messaddeq, M. Dussauze, V. Jubera, T. Cardinal, E. Fargin, Resolved-detrimental surface crystallization in yttrium lanthanum gallate glasses for optical fiber applications, J. Am. Ceram. Soc. (2023) jace.19184, https://doi.org/10.1111/jace.19184.

[24] R. Zaiter, T. Skopak, Y. Ledemi, M. Dussauze, F. Adamietz, E. Fargin, Y. Messaddeq, S. Danto, T. Cardinal, Effect of potassium or yttrium introduction in Yb3+-doped germano-gallate glasses on the structural, luminescence properties and fiber processing, Opt. Mater. 125 (2022), 112070, https://doi.org/10.1016/j.optmat.2022.112070.

[25] J.M. Jewell, P.L. Higby, I.D Aggarwal, Properties of BaO-R2O3- Ga2O3-GeO2 (R = Y, Al, La, and Gd) glasses, J. Am. Ceram. Soc. 77 (3) (1994) 697–700, https://doi.org/10.1111/j.1151-2916.1994.tb05351.x.

[26] R. Zaiter, M. Dussauze, M. Nalin, E. Fargin, F. Adamietz, S. Danto, O. Toulemonde, T. Cardinal, Thermal and structural modification in transparent and magnetic gallogermanate glasses induced by Gd2O3, J. Alloys Compd. 912 (2022), 165181, https://doi.org/10.1016/j.jallcom.2022.165181.

[27] F. Calzavara, M. Allix, M. Dussauze, V. Jubera, M. Nalin, T. Cardinal, E. Fargin, Glass forming regions, structure and properties of lanthanum barium germanate

and gallate glasses, J. Non-Cryst. Solids 571 (2021), 121064, https://doi.org/10.1016/j.jnoncrysol.2021.121064.
[28] L.G. Hwa, Y.R. Chang, W.C. Chao, Infrared spectra of lanthanum gallogermanate glasses, Mater. Chem. Phys. 85 (1) (2004) 158–162, https://doi.org/10.1016/j.matchemphys.2003.12.021.
[29] K. Kowalska, M. Kuwik, J. Pisarska, M. Sitarz, W.A. Pisarski, Raman and infrared spectroscopy of barium-gallo germanate glasses containing B2O3/TiO2, Materials (Basel) 16 (4) (2023) 1516, https://doi.org/10.3390/ma16041516.
[30] G. Tang, D. Zhang, F. Zhang, W. Zhao, Q. Qian, Z. Yang, Structure and luminescence properties of Tm3+ doped barium gallo-germanate glass tailored by Lu2O3, J. Lumin. 257 (2023), 119771, https://doi.org/10.1016/j.jlumin.2023.119771.
[31] G. Tang, D. Yang, W. Huang, X. Song, F. Zhang, Q. Qian, W. Zhao, Z. Yang, Enhanced 2-Mm and upconversion luminescence properties regulated by network structure in Ho $^{3+}$ /Yb $^{3+}$ Co-doped germanate laser glasses, Opt. Lett. 48 (3) (2023) 534, https://doi.org/10.1364/OL.479494.
[32] T. Guérineau, A. Fargues, J. Lapointe, R. Vallée, Y. Messaddeq, L. Canioni, Y. Petit, T. Cardinal, Laser direct writing of silver clusters-based subwavelength periodic structures embedded in mid-infrared Gallo-Germanate glass, Adv. Photon. Res. (2022), 2200032, https://doi.org/10.1002/adpr.202200032.
[33] Q. Zheng, J.C. Mauro, Viscosity of glass-forming systems, J. Am. Ceram. Soc. 100 (1) (2017) 6–25, https://doi.org/10.1111/jace.14678.
[34] K.E. Lipinska-Kalita, FF infrared and laser Raman spectroscopy of amorphous and crystalline germanates, J. Non-Cryst. Solids 119 (1990) 41–48.
[35] J. Alvarado-Rivera, D.A. Rodríguez-Carvajal, M.del C. Acosta-Enríquez, M. B. Manzanares-Martínez, E. Álvarez, R. Lozada-Morales, G.C. Díaz, A. de Leon, M. E. Zayas, Effect of CeO $_2$ on the glass structure of sodium germanate glasses, J. Am. Ceram. Soc. 97 (11) (2014) 3494–3500, https://doi.org/10.1111/jace.13202.
[36] T. Skopak, S. Kroeker, K. Levin, M. Dussauze, R. Méreau, Y. Ledemi, T. Cardinal, E. Fargin, Y. Messaddeq, Structure and properties of gallium-rich sodium germano-gallate glasses, J. Phys. Chem. C 123 (2) (2019) 1370–1378, https://doi.org/10.1021/acs.jpcc.8b08632.
[37] C.I. Merzbacher, D.A. McKeown, X-Ray absorption analysis of Ge and Ga environments in Ba-gallogermante glasses, MRS Proc 307 (1993) 69, https://doi.org/10.1557/PROC-307-69.
[38] D.M. McKeown, C.I. Merzbacher, Raman spectroscopic studies of BaO Ga2O3 GeO2 glasses, J. Non-Cryst. Solids 183 (1–2) (1995) 61–72, https://doi.org/10.1016/0022-3093(94)00648-2.
[39] E.I. Kamitsos, Y.D. Yiannopoulos, M.A. Karakassides, G.D. Chryssikos, H. Jain, Raman and infrared structural investigation of x Rb $_2$ O·(1 − x) GeO $_2$ glasses, J. Phys. Chem. 100 (28) (1996) 11755–11765, doi:10.1021/jp960434+.
[40] K. Fukumi, S.Raman Sakka, Spectroscopic study of the structural role of alkaline earth ions in alkaline earth gallate glasses, J. Non-Cryst. Solids 94 (2) (1987) 251–260, https://doi.org/10.1016/S0022-3093(87)80295-8.
[41] K. Yoshimoto, A. Masuno, I. Sato, Y. Ezura, H. Inoue, M. Ueda, M. Mizuguchi, Y. Yanaba, T. Kawashima, T. Oya, Y. Onodera, S. Kohara, K. Ohara, Principal vibration modes of the La_2O_3 –Ga_2O_3 binary glass originated from diverse coordination environments of oxygen atoms, J. Phys. Chem. B 124 (24) (2020) 5056–5066, https://doi.org/10.1021/acs.jpcb.0c02147.
[42] G.S. Henderson, L.G. Soltay, H.M. Wang, Q speciation in alkali germanate glasses, J. Non-Cryst. Solids 356 (44–49) (2010) 2480–2485, https://doi.org/10.1016/j.jnoncrysol.2010.03.023.
[43] M. Calleri, G. Gazzoni, The structures of (Sr,Ba) I(Al,Ga)z(Si,Ge)2081. III. The crystal structures of the paracelsian- like modifications of synthetic SrGazGezO8 and BaGa2Ge208, Acta. Crystallogr. B. Struct. Sci. Cryst. Eng. Mater. 4 (32) (1976) 1196–1205.
[44] H. Kroll, M.W. Phillips, H. Pentinghaus, The structures of the ordered synthetic feldspars $SrGa_2Si_2O_8$, $BaGa_2Si_2O_8$ and BaGa2Ge2O8, Acta Crystallogr. B34, (1978) 359–365.
[45] G.J. Redhammer, G. Roth, G. Amthauer, Yttrium Pyrogermanate, Y $_2$ Ge $_2$ O $_7$, Acta Crystallogr. C 63 (10) (2007) i93–i95, https://doi.org/10.1107/S0108270107042825.
[46] L.T. Denisova, L.A. Irtyugo, Yu.F. Kargin, V.V. Beletskii, V.M. Denisov, Synthesis and high-temperature heat capacity of Y2Ge2O7, Russ. J. Inorg. Chem. 63 (3) (2018) 361–363, https://doi.org/10.1134/S003602361803004X.
[47] W.H. Zachariasen, The atomic arrangement in glass, J. Am. Chem. Soc. 54 (10) (1932) 3841–3851, https://doi.org/10.1021/ja01349a006.
[48] J.D. Musgraves, J. Hu, L. Calvez (Eds.), Springer Handbook of Glass, Springer Handbooks; Springer International Publishing: Cham, 2019, https://doi.org/10.1007/978-3-319-93728-1.
[49] B. Karmakar, Fundamentals of glass and glass nanocomposites. Glass Nanocomposites, Elsevier, 2016, pp. 3–53, https://doi.org/10.1016/B978-0-323-39309-6.00001-8.
[50] W. Zheng, J. Cheng, L. Tang, J. Quan, X. Cao, Effect of Y2O3 addition on viscosity and crystallization of the lithium aluminosilicate glasses, Thermochim. Acta 456 (1) (2007) 69–74, https://doi.org/10.1016/j.tca.2007.01.022.
[51] W. Zheng, J. Cheng, H. Li, J. Quan, L. Shi, Structure and properties of the lithium aluminosilicate glasses with Yttria addition, J. Wuhan Univ. Technol.-Mater Sci Ed 22 (2) (2007) 362–366, https://doi.org/10.1007/s11595-005-2362-x.
[52] J.E.Scandium Shelby, Yttrium and indium in oxide glasses, Key Eng. Mater. 94–95 (1994) 345–362, https://doi.org/10.4028/www.scientific.net/KEM.94-95.345.
[53] M.J. Pomeroy, E. Nestor, R. Ramesh, S. Hampshire, Properties and crystallization of rare-earth Si-Al-O-N glasses containing mixed trivalent modifiers, J. Am. Ceram. Soc. 88 (4) (2005) 875–881, https://doi.org/10.1111/j.1551-2916.2004.00141.x.
[54] E.A. Mahdy, S. Ibrahim, Influence of Y2O3 on the structure and properties of calcium magnesium aluminosilicate glasses, J. Mol. Struct. 1027 (2012) 81–86, https://doi.org/10.1016/j.molstruc.2012.05.055.
[55] J. Kang, J. Wang, X. Lou, G.A. Khater, Y. Hou, F. Tang, Y. Yue, Effect of Y2O3 content on the crystallization behaviors and physical properties of glasses based on MgO-Al2O3 -SiO2 system, J. Non-Cryst. Solids 497 (2018) 12–18, https://doi.org/10.1016/j.jnoncrysol.2018.05.029.
[56] J. Johnson, R. Weber, M. Grimsditch, Thermal and mechanical properties of rare earth aluminate and low-silica aluminosilicate optical glasses, J. Non-Cryst. Solids 351 (8–9) (2005) 650–655, https://doi.org/10.1016/j.jnoncrysol.2005.01.065.
[57] X. Gao, Q. Zhang, J. Yu, W. Tang, Y. Li, A. Lu, Effect of replacement of Al2O3 by Y2O3 on the structure and properties of alkali-free Boro-aluminosilicate glass, J. Non-Cryst. Solids 481 (2018) 98–102, https://doi.org/10.1016/j.jnoncrysol.2017.10.032.
[58] M. Dittmer, C.F. Yamamoto, C. Bocker, C. Rüssel, Crystallization and mechanical properties of MgO/Al2O3/SiO2/ZrO2 glass-ceramics with and without the addition of Yttria, Solid State Sci 13 (12) (2011) 2146–2153, https://doi.org/10.1016/j.solidstatesciences.2011.09.005.
[59] T. Charpentier, N. Ollier, H. Li, RE2O3-alkaline earth-aluminosilicate fiber glasses: melt properties, crystallization, and the network structures, J. Non-Cryst. Solids 492 (2018) 115–125, https://doi.org/10.1016/j.jnoncrysol.2018.04.028.
[60] N. Bansal, S. Khan, G. Sharma, Rajni, D. Kumar, K Singh, Alkali field strength effects on optical, dielectric, and conducting properties of calcium borosilicate glasses, Ceram. Int. 49 (2) (2023) 2998–3006, https://doi.org/10.1016/j.ceramint.2022.09.284.
[61] I.H. Arita, D.S. Wilkinson, G.R. Purdy, Crystallization of Yttria-alumina-silica glasses, J. Am. Ceram. Soc. 75 (12) (1992) 3315–3320, https://doi.org/10.1111/j.1151-2916.1992.tb04427.x.
[62] Z.H. Xiao, A.X. Lu, C.G. Zuo, Structure and property of multicomponent germanate glass containing Y_2O_3, Adv. Appl. Ceram. 108 (6) (2009) 325–331, https://doi.org/10.1179/174367608X372899.
[63] W. Vogel (Ed.), Glass Chemistry, Springer Berlin Heidelberg, Berlin, Heidelberg, 1994, https://doi.org/10.1007/978-3-642-78723-2.
[64] A. Jaworski, T. Charpentier, B. Stevensson, M. Edén, Scandium and Yttrium environments in aluminosilicate glasses unveiled by $^{45}Sc/^{89}$ Y NMR spectroscopy and DFT calculations: what structural factors dictate the chemical shifts? J. Phys. Chem. C 121 (34) (2017) 18815–18829, https://doi.org/10.1021/acs.jpcc.7b05471.
[65] N.J. Clayden, S. Esposito, A. Aronne, P. Pernice, Solid state 27Al NMR and FTIR study of lanthanum aluminosilicate glasses, J. Non-Cryst. Solids 258 (1–3) (1999) 11–19, https://doi.org/10.1016/S0022-3093(99)00555-4.
[66] P. Florian, N. Sadiki, D. Massiot, J.P Coutures, ^{27}Al NMR study of the structure of lanthanum- and yttrium-based aluminosilicate glasses and melts, J. Phys. Chem. B 111 (33) (2007) 9747–9757, https://doi.org/10.1021/jp072061q.
[67] T. Schaller, J.F. Stebbins, The structural role of lanthanum and yttrium in aluminosilicate glasses: a ^{27} Al and ^{17} O MAS NMR study, J. Phys. Chem. B 102 (52) (1998) 10690–10697, https://doi.org/10.1021/jp982387m.
[68] Q. Zheng, Y. Liu, M. Li, Z. Liu, Y. Hu, X. Zhang, W. Deng, M. Wang, Crystallization behavior and IR structure of yttrium aluminosilicate glasses, J. Eur. Ceram. Soc. 40 (2) (2020) 463–471, https://doi.org/10.1016/j.jeurceramsoc.2019.09.044.
[69] K. Singh, N. Gupta, O.P. Pandey, Effect of Y2O3 on the crystallization behavior of SiO2–MgO–B2O3–Al2O3 glasses, J. Mater. Sci. 42 (15) (2007) 6426–6432, https://doi.org/10.1007/s10853-006-1188-z.